PRAMANA
— journal of
physics

Vol. 62, No. 5
May 2004
pp. 1059–1072

α-Particle induced reactions on rhodium

M S GADKARI and N L SINGH*
Department of Physics, Faculty of Science, M.S. University of Baroda, Vadodara 390 002, India
*Corresponding author
E-mail: msgadkari-poly@mail.msubaroda.ac.in; singhnl_msu@yahoo.com

MS received 31 August 2002; revised 9 January 2004; accepted 17 January 2004

Abstract. Excitation functions for ^{103}Rh $(\alpha, xn); x = 1-4$ and ^{103}Rh $(\alpha, \alpha xn); x = 1-3$ reactions were measured up to 50 MeV bombarding energy using stacked foil activation technique and high purity germanium (HPGe) γ-ray spectroscopy method. The experimental results were compared with calculations considering equilibrium as well as pre-equilibrium hybrid model of Blann (ALICE/90). It is found that the initial exciton configuration $n_0 = 4(4p0h)$ gives fairly good agreements for (α, xn) reactions. There seems to be indication of direct inelastic scattering effects in $(\alpha, \alpha xn)$-type of reactions.

Keywords. Excitation functions; pre-equilibrium effects; γ-ray spectroscopy; stacked foil activation; ALICE/90.

PACS Nos 25.55.-e; 27.60.+j

1. Introduction

The phenomenological models, introduced to describe the emission of fast particles during the equilibration of an excited nucleus, have now become very serviceable tools for the analysis and interpretation of nuclear reactions at energies greater than a few tens of MeV. Nuclear reactions induced by medium energy projectiles are interesting in view of pre-equilibrium and equilibrium de-excitation processes. The highly excited nuclear system produced by the projectile–target interaction decays first by emitting a number of fast nucleons at the pre-equilibrium stage and later on by evaporating low-energy nucleons at the equilibrium stage.

The pre-equilibrium process has been extensively studied since the exciton model was proposed by Griffin [1]. However, the two completely different reaction theories [2] have to be linked together for obtaining a satisfactory description of the experimental results. The success of the simple formulations used rests in the use of a statistical assumption applied to each configurational hierarchy as denoted by the exciton number, i.e., the number of excited particles plus holes. The initial exciton number (n_0) characterizes the initial excitation energy distribution engendered by

the projectile entering the target nucleus at the start. The various pre-equilibrium theories differ appreciably in their flexibility and in mathematical rigour. The semi-classical theories [3–9] have been applied to a much wider range of reactions than the quantum mechanical theories [10–13], in particular, to those initiated by complex particles and those leading to the emission of many particles. By contrast, the quantum mechanical theories have so far been confined to nucleon interactions with not more than two emergent particles. For the interaction of a complex particle like an α-particle the quantum mechanical picture is yet to come.

Though the cross-sections for α-particle induced reactions on rhodium were measured by several groups [14–17], there are mutual discrepancies among their results. Hence precise and accurate measurements are still needed. Keeping this in mind, we have made a systematic study of the excitation function of α-particle induced reactions on rhodium up to 50 MeV. One of the objectives of the present study is to test the pre-equilibrium hybrid model (ALICE/90).

2. Experimental procedure

The excitation functions for α-particle induced reactions on rhodium were measured by the stacked foil activation technique and high purity germanium (HPGe) γ-ray spectroscopy method up to 50 MeV.

2.1 *Preparation of target stack*

Spectroscopically pure (99.99%) rhodium foils of 14.88 mg/cm^2 thickness were taken and a stack of ten such foils was prepared which was used as a target. The samples were cut into pieces of 1.2 × 1.2 cm^2 each and glued on aluminum frame of size 3 × 2.5 cm^2 having a circular hole of 8 mm diameter in its centre. The aluminum foils of varying thicknesses were also inserted in the stack which acted as energy degraders. The beam energy was degraded down to about 16 MeV. After accounting for the energy degradation in the aluminum foils, the energy of the α-beam at half the thickness of the rhodium foil was calculated from range energy tables of Hubert *et al* [18].

2.2 *Irradiation and counting*

The stack was irradiated at Variable Energy Cyclotron Centre (VECC), Kolkata, India using 50 MeV α-particles. The beam spot on the foil stack was restricted to 5 mm by a central hole in a 6 mm thick tantalum collimator placed in front of the stack. The α-beam were totally stopped in the electrically insulated irradiation head serving as a kind of Faraday cup where secondary electrons were prevented from escaping. A beam current of the order of 200 nA was maintained in the stack for 2.4 h. During the irradiation, low conductivity water (LCW) was circulated through specially designed jet assembly, which cooled both the flange as well as the stack. The incident α-particle flux was calculated by measuring the activities of

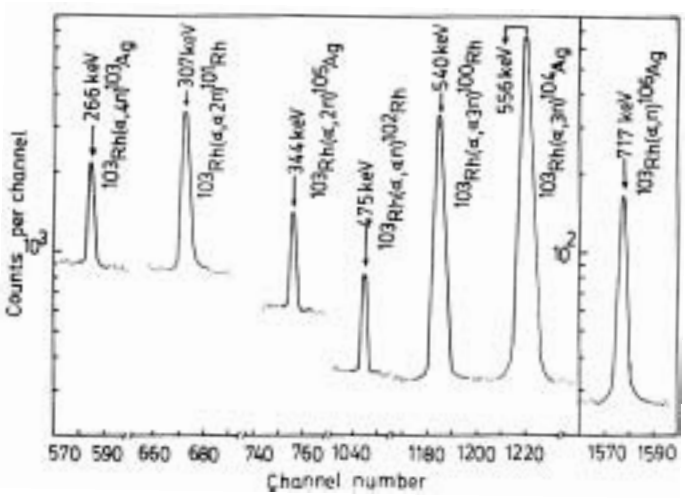

Figure 1. A typical γ-ray spectrum of activated sample of rhodium at 38.0 MeV.

^{24}Na in the reaction $^{27}\mathrm{Al}(\alpha, \alpha 2pn)^{24}\mathrm{Na}$, for which well-measured cross-sections are available in the literature [19]. The charge collected in the Faraday cup was also used to calculate the average flux of the incident α-beam. In general, the two values agreed within 5%. The activities produced in each foil were measured using a 120 cc HPGe detector having a resolution of 2 keV for 1332 keV photons of ^{60}Co, coupled with a 4096 channel analyser. Several spectra were taken at suitable intervals to permit identification of the half-lives of various residual nuclei. A typical γ-ray spectrum obtained from the activation of rhodium target foil at 38 MeV is shown in figure 1. The energy calibration and efficiency of the detector were determined with a ^{152}Eu standard source obtained from the Radio-chemistry Laboratory at VECC, Kolkata. The residual nuclei were identified and their yields measured using their characteristic γ-rays mentioned in table 1 [20].

2.3 *Formulation*

The formula used for the determination of cross-section is reported in our earlier paper [21].

$$\sigma = \frac{A_i A_\gamma \lambda(\mathrm{e}^{\lambda t_w})}{\phi \theta_\gamma P_\gamma \omega_i N_{\mathrm{av}} (1 - \mathrm{e}^{-\lambda t_i})(1 - \mathrm{e}^{-\lambda t_c})}, \tag{1}$$

where σ is the cross-section for the reaction, A_i is the gram atomic weight of the target element, A_γ is the area under photopeak of characteristic γ-ray of the residual nucleus, λ is the disintegration constant of the product nucleus, ϕ is the flux of the incident particle, θ_γ is the absolute γ-ray intensity per decay of the residual nucleus, P_γ is the photopeak efficiency of the γ-ray, ω_i is the weight per unit area of the target foil, N_{av} is the Avogadro number, t_i is the time of irradiation, t_w is the

Table 1. Nuclear data used for the identification of residual nuclei [20].

Reaction	Q-value (MeV)	$T_{1/2}^{\cdot}$	E_γ (keV)	θ_γ (%)
^{103}Rh$(\alpha, n)^{106\mathrm{m}}$Ag	−6.8	8.5 d	616	21.6
			717	29.1
			748	20.7
			824	15.4
^{103}Rh$(\alpha, n)^{106\mathrm{g}}$Ag	−6.7	24.0 m	512	17.0
^{103}Rh$(\alpha, 2n)^{105\mathrm{m}}$Ag	−14.7	7.2 m	319	0.16
^{103}Rh$(\alpha, 2n)^{105\mathrm{g}}$Ag	−14.6	41.2 d	280	31.1
			344	42.7
			443	12.0
			644	11.9
^{103}Rh$(\alpha, 3n)^{104\mathrm{m}}$Ag	−24.6	33.5 m	556	60.0
			767	0.6
			786	2.4
			1238	1.2
^{103}Rh$(\alpha, 3n)^{104\mathrm{g}}$Ag	−24.6	69.2 m	556	91.0
			767	65.0
			857	10.1
			925	12.2
			941	24.6
^{103}Rh$(\alpha, 4n)^{103\mathrm{m}}$Ag	−33.2	5.7 s	134	21.0
^{103}Rh$(\alpha, 4n)^{103\mathrm{g}}$Ag	−33.0	1.1 h	244	6.0
			266	9.4
			531	6.1
^{103}Rh$(\alpha, \alpha n)^{102\mathrm{g}}$Rh	−9.3	206.0 d	475	45.0
			628	4.4
^{103}Rh$(\alpha, \alpha 2n)^{101\mathrm{m}}$Rh	−16.9	4.34 d	307	87.0
			544	4.0
^{103}Rh$(\alpha, \alpha 3n)^{100}$Rh	−26.6	20.8 h	446	11.1
			540	78.0
			588	4.1
			822	20.1
Monitor reaction				
^{27}Al$(\alpha, \alpha 2pn)^{24}$Na	−31.4	15.05 h	1369	100.0

time between the end of irradiation and beginning of counting and t_c is the data collection time (or counting time). The factor $(A_\gamma \lambda e^{\lambda t_w})/(1 - e^{-\lambda t_c})$ is the count rate of the induced activity just at the end of irradiation.

2.4 *Experimental errors*

The overall errors in the presently measured cross-sections are subdivided into the following categories:

(i) In order to estimate the number of nuclei in the target and to check the thickness and uniformity of the sample, pieces of sample foils were weighed on an electronic micro-balance and the thickness of each foil was calculated. This non-uniformity in the foil thickness introduces 1 to 2% error (δ_1).

(ii) Variation in the incident α-particle flux introduces some uncertainty in the final calculation of the cross-sections. In the present experiment the standard monitor cross-sections were taken from literature [19] in the flux determination. This introduces an overall error of 6% (δ_2).

(iii) The calculated detection efficiency may be inaccurate owing to the uncertainty in the spectroscopic data of the standard source and the statistical errors in the counts. No corrections were applied for the uncertainty in the spectroscopic data. However, the statistical error in the counting of the standard ^{152}Eu γ-source used for the efficiency calculation was estimated to be around 3–4% (δ_3).

(iv) The dead time in the pulse processing electronics leads to a loss of counts. The sample–detector distance was suitably adjusted to keep the dead time low (<5%) and corrections for it were applied accordingly in the counting rates.

However, the error introduced in the determination of photopeak areas of the characteristic γ-rays were within the limits of 1 to 4% in the best and worst cases (δ_4).

Therefore the total absolute error in the measured cross-section is

$$\sqrt{\sum_{i=1}^{4}(\delta_i)^2}$$

and found to vary between 7 and 9% for the best and the worst cases. The above-mentioned errors in the measurement of experimental cross-sections do not include the uncertainty of the nuclear data (e.g. half-lives of residual nuclei, branching ratio etc.) that were taken from the table of isotopes [20].

3. Experimental results

In the present work, we have measured the cross-sections for ^{103}Rh $[(\alpha, n); (\alpha, 2n); (\alpha, 3n); (\alpha, 4n); (\alpha, \alpha n); (\alpha, \alpha 2n)$ and $(\alpha, \alpha 3n)]$ reactions by detecting characteristic γ-rays obtained from the decay of residual nuclei. In the present measurement, we have considered only those γ-rays that gave appreciable activities for the meaningful studies. The measured cross-sections have been listed in table 2.

3.1 *Excitation functions for the reactions* $^{103}\mathrm{Rh}(\alpha, xn)$; $x = 1$–4

The residual nucleus ^{106}Ag produced through $^{103}\mathrm{Rh}(\alpha, n)$ reaction has two isomers $^{106\mathrm{m}}$Ag ($T_{1/2}$ = 8.5 d) and $^{106\mathrm{g}}$Ag ($T_{1/2}$ = 24 min) respectively. Both the states

Table 2. Cross-sections of the α-induced reactions on ^{103}Rh.

Reaction	(α, n)	$(\alpha, 2n)$	$(\alpha, 3n)$	$(\alpha, 4n)$	$(\alpha, \alpha n)$	$(\alpha, \alpha 2n)$	$(\alpha, \alpha 3n)$
Product nucleus	^{106m}Ag	^{105}Ag	^{104}Ag	^{103}Ag	^{102m}Rh	^{101m}Rh	^{100}Rh
Threshold energy (MeV)	7.0	15.2	25.6	34.3	9.6	17.5	27.6
E_α (MeV)	σ (mb)	σ (mb)	σ (mb)	σ (mb)	σ (mb)	σ (mb)	σ (mb)
17.6±1.2	128±10	129±10					
21.5±1.1	76.0±6.0	553±42					
25.0±1.0	28.0±2.0	856±66					
28.4±1.0	13.2±1.0	873±68	114±9		30.5±2.4	0.9±0.0	
31.4±0.8	8.1±0.7	650±50	554±42		51.5±4.0	1.3±0.1	
34.4±0.8	5.8±0.5	331±25	988±74		80.0±6.3	11.1±0.9	
38.0±0.8	4.6±0.4	149±11	1078±81	64.0±5.0	89.0±7.0	31.6±2.5	
41.5±0.7	3.5±0.3	89.0±7.0	648±33	235±18	98.0±8.0	51.0±4.0	0.4±0.0
44.9±0.7	2.8±0.3	61.0±4.7	422±32	477±36	101±8	58.0±4.5	10.9±0.8
47.8±0.6	2.5±0.2	47.0±3.6	260±20	630±48	103±8	57.0±4.5	31.5±2.5

decay independently to the ground state. The state ^{106g}Ag ($T_{1/2} = 24$ min) has a single γ-ray of energy 512 keV which is very close to annihilation peak at 511 keV. Therefore, we have measured only partial cross-sections by measuring the activity of ^{106m}Ag.

The residual nucleus ^{105}Ag produced through ^{103}Rh$(\alpha, 2n)$ reaction exists in two states. The metastable state ^{105m}Ag ($T_{1/2} = 7.23$ min) decays completely through isomeric transition (100%) to the ground state ^{105g}Ag ($T_{1/2} = 41.29$ d). In this case the total cross-section was measured by allowing for complete decay of the metastable state to the ground state.

The residual nucleus ^{104}Ag produced through ^{103}Rh$(\alpha, 3n)$ reaction exists in two states. The metastable state ^{104m}Ag ($T_{1/2} = 33.5$ min) decays by electron capture along with β^+ decay (99.93%). In this case, the partial cross-section was measured by measuring the activity of ^{104g}Ag after a complete decay of metastable state.

In the reaction ^{103}Rh$(\alpha, 4n)$, the residual nucleus ^{103}Ag exists in two states. The metastable state ^{103m}Ag ($T_{1/2} = 5.7$ s) decays completely to the ground state ^{103g}Ag ($T_{1/2} = 1.1$ h) through an isomeric transition (100%). In this case the total cross-section was measured by allowing for the complete decay of the metastable state to the ground state.

3.2 *Excitation function for the reactions* ^{103}Rh$(\alpha, \alpha xn)$; $x = 1$–3

In the reaction ^{103}Rh$(\alpha, \alpha n)^{102}$Rh, the ground state ^{102g}Rh is having a long half-life (i.e. $T_{1/2} = 2.9$ yr) and hence it was not measured while ^{102m}Rh ($T_{1/2} = 206$ d) measured in the present work decays to the ground state almost independently through electron capture (80%) and β^+ decay (20%).

In the reaction ^{103}Rh$(\alpha, \alpha 2n)^{101}$Rh, the ground state ^{101g}Rh has a long half-life (i.e. $T_{1/2} = 3.3$ yr) and was not measured while ^{101m}Rh ($T_{1/2} = 4.3$ d) measured in the present work decays to the ground state almost independently through electron

capture (92.8%). Therefore, in both these reactions, the partial cross-sections were measured by measuring the activities of the metastable states.

The residual nucleus ^{100}Rh produced through ^{103}Rh$(\alpha, \alpha 3n)$ reaction has two isomers ^{100m}Rh ($T_{1/2}$ = 4.7 min) and ^{100g}Rh ($T_{1/2}$ = 20.8 h) respectively. The decay of metastable state to the ground state is mostly through isomeric transition (98.3%) and remaining through electron capture along with β^+ decay. In this case the total cross-section was measured by allowing for complete decay of metastable state to the ground state.

4. Model calculations

The excitation functions have been calculated theoretically using the statistical model with and without the inclusion of pre-equilibrium emission of particles. We have used the code ALICE/90 based on the updated version of hybrid model [6] code ALICE/85/300 [21], in which a shell-dependent level density formula of Kataria *et al* [22] is incorporated. A short description of the options chosen is given below.

The nuclear masses were calculated from the Myers–Swiatecki mass formula [23] considering the liquid drop with shell correction term and without pairing. The inverse cross-sections were calculated using the optical model subroutine included in the code that uses the Becchetti and Greenless [24] optical model parameters. The intranuclear transition rates are calculated from the imaginary part of the optical model potential. The equilibrium part was calculated using standard Weisskopf and Ewing [25] formalism. The mean free path multiplier k was kept equal to unity. The mean free path, which is a kind of free parameter, was introduced by Blann [26] to account for the transparency of nuclear matter in the lower density nuclear periphery. A level density parameter $a = A/9$ MeV^{-1} was used.

A crucial parameter in the model is the initial exciton number n_0, defined as $n_0 = p_0 + h_0$ with $p_0 = p_\pi + p_\nu$, where p_0 and h_0 are initially excited particles above and holes below the Fermi level; p_π and p_ν are the number of protons and neutrons among the excited particles. It is customary to use the initial exciton number n_0 $(p_0 h_0)$ as a fit parameter to match the theoretical predictions with the experimentally observed shape of the spectra and excitation functions. The initial exciton number n_0 governs the entire cascading process of binary collisions and thereby influences the shape of the hard component in the particle spectra and high energy tail in the excitation functions. A good guess would be the number of nucleons in the projectile or an additional particle/hole or both. For an incident α-particle used in the present work, a reasonable choice for the initial exciton number is $n_0 = 4, 5$ and 6 using different initial exciton configurations such as $(4p0h), (5p0h)$ and $(5p1h)$ respectively. We performed the calculations using the above exciton configurations and it was found that $n_0 = 4(4p0h)$ gives by far the best results beyond the equilibrium than the other two configurations. The predictions of $n_0 = 5(5p0h)$ and $n_0 = 6(5p1h)$ configurations were lower than those of $n_0 = 4(4p0h)$ [2,27].

5. Results and discussion

Figures 2–8 show the present experimental results together with the previous results [14–17] wherever available. In figures 2–7, the present results are shown by dark circles and the vertical bars represent the total estimated errors in the cross-sections. If no bar is depicted, the size of the circle includes the magnitude of the statistical errors.

Hansen and Stelts [14] in 1964 studied ^{103}Rh(α, n) reaction in the energy range of 12–18 MeV using polyethylene 'long counters' with an overall error of 10%. Ozafran *et al* [15] in 1980 determined excitation functions for ^{103}Rh$[(\alpha, n), (\alpha, 2n), (\alpha, 3n), (\alpha, 4n), (\alpha, \alpha 3n), (\alpha, \alpha 4n)]$ reactions in the energy range of 10–55 MeV using Ge-intrinsic solid state detector. The overall error in the measurement was 7–8%. Newton *et al* [16] in 1981 measured excitation functions for $(\alpha, n), (\alpha, 2n), (\alpha, 3n), (\alpha, 4n)$ and $(\alpha, 5n)$ reactions on ^{103}Rh in the energy range of 18–38 MeV and 36–82 MeV using Ge(Li) detector. In this case the target was prepared by electroplating rhodium film on copper foil. However, error in the measurement was not mentioned. Ansari *et al* [17] in 1996 measured the excitation functions for $(\alpha, n), (\alpha, 2n)$ and $(\alpha, 3n)$ reactions on ^{103}Rh in the energy range of 10–40 MeV using Ge(Li) detector with an estimated error up to 16%.

The experimental excitation functions were also compared with the theoretical predictions based on equilibrium and pre-equilibrium reaction mechanism. Comparison with the theory is made only for those reactions in which the total cross-section was measured in the present work. In the figures, the pre-equilibrium hybrid model predictions are shown by solid line and the Weisskopf–Ewing estimates by the dashed line. The lines are drawn only to guide the eye.

5.1 ^{103}Rh(α, n) *reaction*

The excitation functions for (α, n) reaction are shown in figure 2 together with the previous results. It is evident from the figure that the results of Hansen and Stelts constitute only the initial rising part of the excitation function and are overestimated by a factor of 10 in the peak region of the excitation function. The present results are in good agreement with the results of Newton *et al* which are in the energy region up to 25 MeV. The present results are also in fair agreement with the results of Ansari *et al* in the overlapping region of energies. However, it is evident from the figure that the results of Ozafran *et al* are underestimated by a factor of two as well as they show a shift of about 6 MeV towards the high-energy side at peak position. Since we have measured the partial cross-sections by measuring the activities in the metastable state only, the present results are not compared with the theory.

5.2 ^{103}Rh$(\alpha, 2n)$ *reaction*

The excitation functions for $(\alpha, 2n)$ reaction are shown in figure 3 together with the previous results as well as theoretical predictions based on Weisskopf–Ewing (WE)

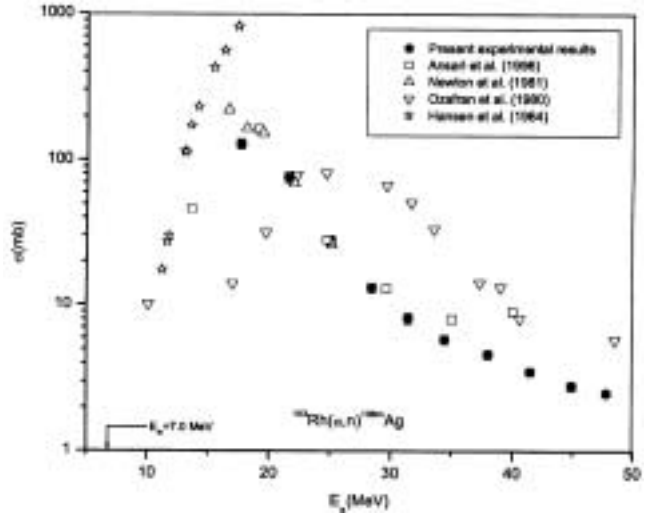

Figure 2. Experimental excitation function of $^{103}\mathrm{Rh}(\alpha, n)^{106\mathrm{m}}\mathrm{Ag}$ reaction.

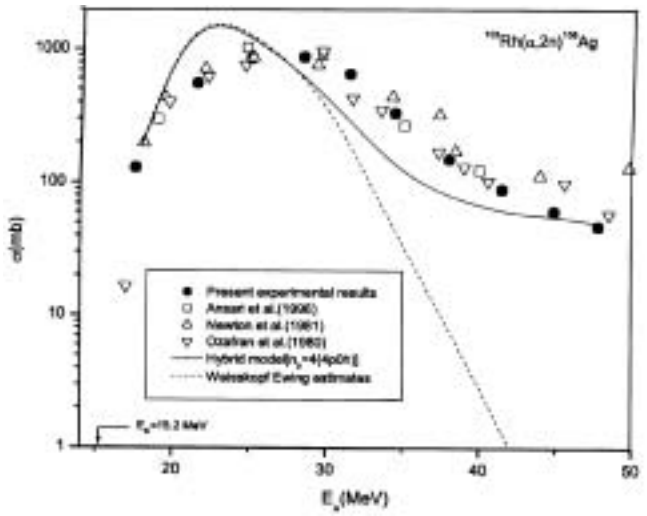

Figure 3. Experimental and theoretical excitation of $^{103}\mathrm{Rh}(\alpha, 2n)^{105}\mathrm{Ag}$ reaction.

estimates giving compound nucleus contributions as well as pre-equilibrium hybrid model predictions using initial exciton configuration $n_0 = 4(4p0h)$. It is evident from the figure that the present results are in general agreement with the previous measurements and are very systematic in the entire region of energy. Further, it is observed that the WE estimates accounted well the low-energy compound nucleus dominated part of the excitation function but failed to account for the observed tail at high energies where non-equilibrium effects predominate beyond a few tens

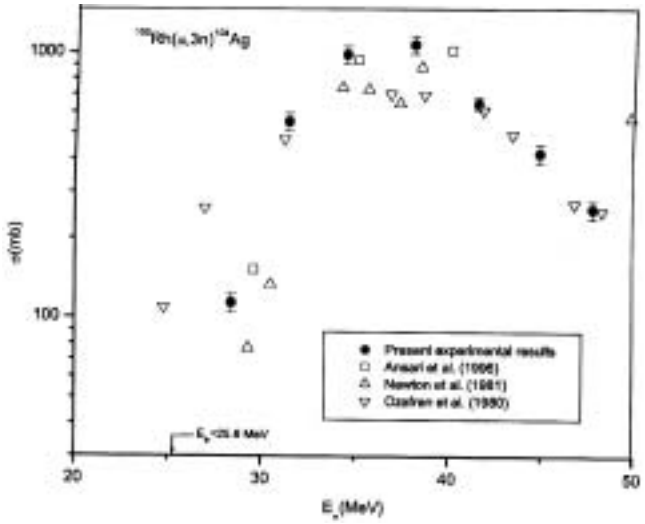

Figure 4. Experimental excitation function of $^{103}\mathrm{Rh}(\alpha, 3n)^{104}\mathrm{Ag}$ reaction.

of MeV of bombarding energy. The high-energy region of the excitation function is accounted well by hybrid model predictions using initial exciton configuration $n_0 = 4(4p0h)$, i.e., pure particle state.

5.3 $^{103}\mathrm{Rh}(\alpha, 3n)$ *reaction*

The excitation functions for $(\alpha, 3n)$ reactions are shown in figure 4 together with the previous results. It is seen from the figure that the present results are in good agreement with the results of Ansari *et al*. However, the results of Ozafran *et al* are overestimated by a factor of two in the initial rising part of the excitation function but they are in fair agreement with the present results in the high-energy region. The results of Newton *et al* are underestimated by a factor of four in the lower energy region whereas the same are overestimated by a factor of four in the higher energy region. Since we have not measured the total cross-section in the present case, it is not appropriate to compare our results with the theory.

5.4 $^{103}\mathrm{Rh}(\alpha, 4n)$ *reaction*

The excitation functions for $(\alpha, 4n)$ reaction are shown in figure 5 along with previous experimental results as well as theoretical predictions based on Weisskopf–Ewing estimates giving compound nucleus contribution and pre-equilibrium hybrid model predictions using initial exciton configuration $n_0 = 4(4p0h)$. It is evident from the figure that the results of Ozafran *et al* are overestimated whereas the results of Newton *et al* are underestimated by a factor of about 3–5 in the energy region 35–45 MeV. The threshold energy for the $\mathrm{Rh}(\alpha, 4n)$ reaction is rather large

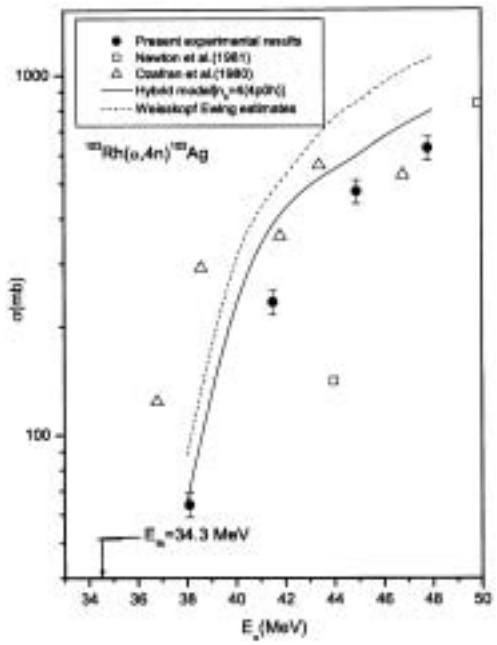

Figure 5. Experimental and theoretical excitation functions for ^{103}Rh $(\alpha, 4n)^{103}$Ag reaction.

(34.3 MeV) and as such there are few data points only in the initial rising part of the excitation function. In this region, the pre-equilibrium model predictions are not very sensitive as the compound nucleus mechanism still dominates. But it can be seen that the theoretical predictions taking into account the pre-equilibrium contribution are comparatively closer to the presently measured results.

5.5 ^{103}Rh$(\alpha, \alpha n)$ *and* ^{103}Rh$(\alpha, \alpha 2n)$ *reactions*

The excitation functions for $(\alpha, \alpha n)$ and $(\alpha, \alpha 2n)$ reactions are shown in figure 6 and figure 7 respectively. Any earlier measurement is not available in the case of these two reactions. Also, in the case of Rh$(\alpha, \alpha n)$ and Rh$(\alpha, \alpha 2n)$ reactions, the partial cross-sections for the genetically independent isomeric states were not measured in the present work. These states have their half-lives in years which were not measured. The observed shape of experimental excitation functions strongly suggests the influence of direct interaction effects in the emission of α-particles. The observed slowly rising monotonous shape, particularly for $(\alpha, \alpha xn)$ type of reactions, points out to a possible inelastic scattering of the incident α-particles, followed by neutron evaporation. Similar observations were made by Lanzafame and Blann [28] while studying α-particle induced reactions on gold. They studied the recoil ranges of the residual nuclei in $(\alpha, \alpha xn)$ type of the reactions and found that there is a very little momentum transfer to the recoiling nucleus as expected for a direct interaction.

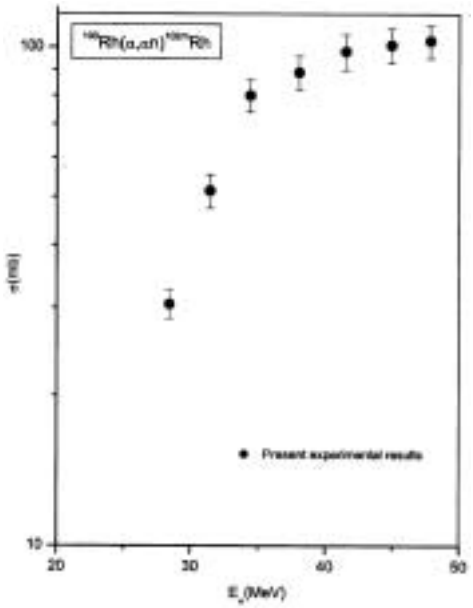

Figure 6. Experimental excitation function of $^{103}\mathrm{Rh}(\alpha, \alpha n)^{102\mathrm{m}}\mathrm{Rh}$ reaction.

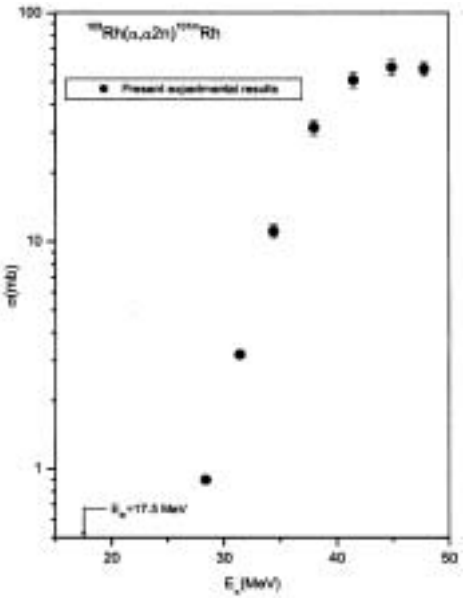

Figure 7. Experimental excitation function of $^{103}\mathrm{Rh}(\alpha, \alpha 2n)^{101\mathrm{m}}\mathrm{Rh}$ reaction.

5.6 $^{103}\mathrm{Rh}(\alpha, \alpha 3n)$ *reaction*

The excitation functions for $(\alpha, \alpha 3n)$ reactions are shown in figure 8 together with the previous results. The threshold energy for $\mathrm{Rh}(\alpha, \alpha 3n)$ reaction is rather large (26.6 MeV) and as such there are only three data points in the initial rising part of the experimental excitation function. Therefore it is not appropriate to compare our results with the theory.

6. Conclusions

Excitation functions for Rh[(α, n); $(\alpha, 2n)$; $(\alpha, 3n)$; $(\alpha, 4n)$; $(\alpha, \alpha n)$; $(\alpha, \alpha 2n)$; $(\alpha, \alpha 3n)$] reactions were studied up to 50 MeV. From the overall comparison between the present and previous experimental results, it is quite evident that there are large mutual discrepancies among the previously measured values. From figures 2–7, it is clear that the present measurements are more systematic than the previously measured values.

From an overall comparison between experimental results and theoretical predictions based on compound nucleus Weisskopf–Ewing estimates as well as preequilibrium hybrid model, one can infer that Weisskopf–Ewing estimates accounted fairly well the low-energy compound nucleus dominated part of the excitation functions for $(\alpha, 2n)$ and $(\alpha, 4n)$ reactions but failed to account the observed cross-sections in the case of $(\alpha, 2n)$ reaction at higher energies, where non-equilibrium

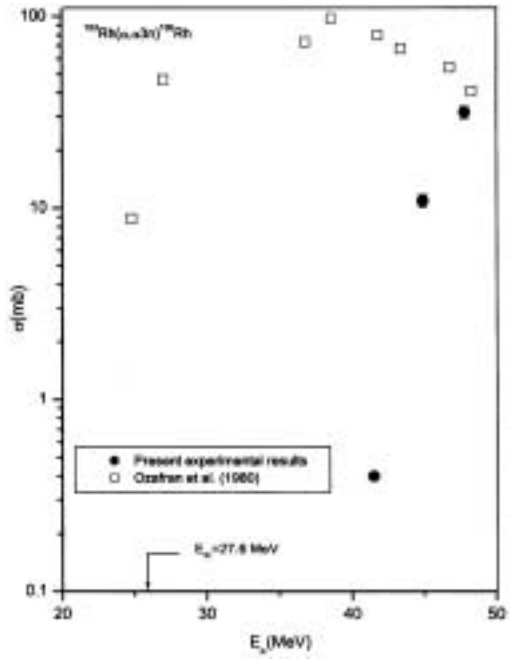

Figure 8. Experimental excitation function of $^{103}\mathrm{Rh}(\alpha, \alpha 3n)^{100}\mathrm{Rh}$ reaction.

effects predominate beyond a few tens of MeV of bombarding energy. The hybrid model gives a fairly good account of nucleon emission with an initial exciton number $n_0 = 4(4p0h)$, which is separated in the case of proton and neutron excitons (n_p and n_n respectively) above and hole (n_h) below the Fermi level, and the best fit is obtained with $n_\mathrm{p} = 2, n_\mathrm{n} = 2$ and $n_\mathrm{h} = 0$ that is pure particle state. This picture is quite consistent with the basic physics of pre-equilibrium decay that only a small number of degrees of freedom are initially excited in a nuclear reaction at moderate energies. However, in the case of (α, n), $(\alpha, 3n)$, $(\alpha, \alpha n)$ and $(\alpha, \alpha 2n)$ reactions, partial cross-sections for the isomeric states were not measured. Since the theoretical code [21] provides the total cross-section of the reaction, these experimental excitation functions are not compared with the theoretical predictions. Further, it may be speculated that for $(\alpha, \alpha x n)$ type of reactions, with small neutron multiplicity, a direct inelastic scattering followed by neutron evaporation could be a contributing factor.

Acknowledgements

The authors are thankful to the entire staff of Inter-University Consortium for Department of Atomic Energy Facilities (IUC-DAEF), Kolkata Centre and Variable Energy Cyclotron Centre, Kolkata, India for their efforts for the successful completion of the experimental programme. The financial support by IUC-DAEF Kolkata Centre is gratefully acknowledged.

References

[1] J J Griffin, *Phys. Rev. Lett.* **17**, 478 (1966)
[2] M Blann, *Annu. Rev. Nucl. Sci.* **25**, 123 (1975)
[3] G D Harp, J M Miller and B J Berne, *Phys. Rev.* **165**, 1166 (1968)
[4] M Blann, *Phys. Rev. Lett.* **27**, 337 (1971); **27**, 700E (1971); **27**, 1550E (1971)
[5] E Gadioli, E Gadioli-Erba and P G Sona, *Nucl. Phys.* **A271**, 589 (1973)
[6] M Blann and H K Vonach, *Phys. Rev.* **C28**, 1475 (1983)
[7] J Ernst, W Friedland and H Stockhorst, *Z. Phys.* **A328**, 333 (1987)
[8] G Mantzouranis, D Agassi and H A Weidenmüeller, *Z. Phys.* **A27**, 145 (1976)
[9] J M Akkermans, H Gruppelaar and G Reffo, *Phys. Rev.* **C22**, 73 (1980)
[10] D Agassi, H A Weidenmüeller and G Mantzouranis, *Phys. Rev.* **C22**, 145 (1975)
[11] T Tamura, T Udagawa, D H Feng and K K Kan, *Phys. Lett.* **B68**, 109 (1977)
[12] L Avaldi, R Bonetti and L Colli Milazzo, *Phys. Lett.* **B94**, 463 (1980)
[13] G M Field, R Bonetti and P E Hodgson, *J. Phys.* **G12**, 93 (1986)
[14] L F Hansen and M L Stelts, *Phys. Rev.* **136**, 1000 (1964)
[15] M J Ozafran, M E Vazquez, M De La Vega Vedoya and S J Nassiff, *Radiochem. Radional. Lett.* **43**, 265 (1980)
[16] G W A Newton, V J Robinson and E M Shaw, *J. Inorg. Nucl. Chem.* **43**, 2227 (1981)
[17] M Afzal Ansari, N P M Sathik, B P Singh, M G V Sankaracharyulu and R Prasad, *Int. J. Mod. Phys.* **E5**, 345 (1996)
[18] F Hubert, R Bimbot and H Gauvin, *Atomic Data Nucl. Data Tables* **46**, 96 (1990)
[19] H J Probst, S M Qaim and R Weinreich, *Int. J. Appl. Rad. Isotopes* **27**, 431 (1976)
[20] C M Lederer and V S Shirley, *Table of isotopes*, 7th edition (John Wiley & Sons, New York, 1978)
[21] M Blann, Code ALICE/85/300, Lawrence Livermore National Laboratory Report UCID-20169, unpublished (1984)
[22] S K Kataria, V S Ramamurthy and S S Kapoor, *Phys. Rev.* **C18**, 549 (1978)
[23] W D Myers and W J Swiatecki, *Ark. Fys.* **36**, 343 (1967)
[24] F D Becchetti and G W Greenless, *Phys. Rev.* **182**, 1190 (1969)
[25] V F Weisskopf and D H Ewing, *Phys. Rev.* **57**, 472 (1940)
[26] M Blann, *Phys. Rev. Lett.* **27**, 337 (1971)
[27] N L Singh, M S Gadkari and S N Chintalapudi, *Phys. Scr.* **61**, 550 (2000)
[28] F M Lanzafame and M Blann, *Nucl. Phys.* **A142**, 545 (1970)